Stability properties of solitary waves and periodic wave trains in a two-dimensional network of spiking neurons

Werner M. Kistler*
Swiss Federal Institute of Technology-Lausanne, EPFL, 1015 Lausanne, Switzerland
(Received 5 April 2000)

We investigate solitary waves of excitation in a two-dimensional network of spiking neurons with distance-dependent couplings. A continuum description is developed that does not require spatial or temporal averaging. Using this description, propagation velocities and dispersion relations for solitary waves and periodic wave trains can be calculated analytically. We show that the stability properties of solitary waves and wave trains are dominated by form instabilities which are genuine to the two-dimensional nature of the system.

PACS number(s): 87.18.Pj, 05.45.Yv, 84.35.+i

Traveling waves are an intensely studied phenomenon as they occur in a large class of different systems—collectively termed excitable media—that range from physico-chemical reaction-diffusion (RD) systems to biological tissues such as muscle cells or neuronal networks. Several authors have studied the evolution of neuronal activity in spatially extended but locally connected networks using either simulations of biophysical models [1–3] or simplified mathematical models [4–7]. Mathematical models are usually based on a continuum approximation that relies on a temporal and spatial coarse-graining of the microscopic variables [4]. Recently, there has been growing interest in a slightly different class of models that describes the neuronal dynamics directly in terms of individual action potentials instead of an average firing rate and thus does without temporal coarse-graining [8–12]. Here we show that a continuum approximation can be achieved even without averaging spatially. The continuum model yields the same results as the underlying discrete model provided that the synaptic coupling strength is a slowly varying function of the neuronal distance.

We consider a network of spiking neurons arranged on a two-dimensional grid. Each neuron is described by the spike response model which is basically an integrated version of the integrate-and-fire model [13–15]. The membrane potential $V_i(t)$ of neuron i is given by

$$V_i(t)=\sum_j J_{ij}\int_{-\infty}^{t} dt'\,\epsilon(t-t')S_j(t') + \int_{-\infty}^{t} dt'\,\eta(t-t')S_i(t'), \tag{1}$$

with $S_j(t)=\Sigma_f \delta(t-t_j^f)$ being the spike train of neuron j, where each spike at firing time t_j^f is represented by a Dirac pulse. The response of the membrane to an incoming action potential is described by means of a scalar J_{ij} that is the synoptic coupling strength, and a function ϵ that has the form of a typical postsynaptic potential, e.g., $\epsilon(t)=(t/\tau^2)\exp(-t/\tau)\Theta(t)$ with Θ being the Heaviside step-function. Refractoriness is taken into account by adding a (negative) afterpotential η whenever the neuron has fired. An action potential is triggered as soon as the membrane potential reaches the firing threshold ϑ from below, i.e.,

$$S_i(t)=\delta[V_i(t)-\vartheta]\left[\frac{d}{dt}V_i(t)\right]_+. \tag{2}$$

Here, $[\cdot]_+$ denotes the positive part of the argument. This factor is necessary in order to produce a normalized δ function in time whenever the threshold is crossed with positive slope.

A topology is induced on the set of neurons by assigning a spatial location $\boldsymbol{r}_i\in\mathbb{R}^2$ to each neuron i. We will assume homogeneous and isotropic synaptic couplings, i.e., couplings $J_{ij}=J(r_{ij})$ that depend on the distance r_{ij} of two neurons. To be specific, we will use a ''Mexican hat''−type interaction with excitation between nearby neurons and a weak inhibition between distant neurons, e.g.,

$$J(r)=a_1\exp(-r^2/\rho_1^2)-a_2\exp(-r^2/\rho_2^2), \tag{3}$$

with $a_1>a_2>0$ and $\rho_1^2<\rho_2^2$ [8].

For the sake of simplicity we assume that the neurons are distributed on a square lattice, e.g., $\boldsymbol{r}_i\in\mathbb{Z}^2$, and that each point of the lattice contains exactly one neuron so that each neuron is uniquely characterized by its spatial coordinates. We can thus rewrite the membrane potential $V_i(t)$ of neuron i at position $\boldsymbol{r}_i$ as $V(\boldsymbol{r}_i,t)$ and, similarly, the spike train $S_i(t)$ as $S(\boldsymbol{r}_i,t)$. Both the membrane potential $V(\boldsymbol{r}_i,t)$ and the spike train $S(\boldsymbol{r}_i,t)$ are now functions of spatial and temporal variables, but, for the time being, the dependency upon the spatial variable is defined only for points on the grid. With this notation the equations of motion 1 and 2 are of the form

$$V(\boldsymbol{r},t)=\sum_j J(\|\boldsymbol{r}-\boldsymbol{r}_j\|)\int_{-\infty}^{t} dt'\,\epsilon(t-t')S(\boldsymbol{r}_j,t') + \int_{-\infty}^{t} dt'\,\eta(t-t')S(\boldsymbol{r},t'), \tag{4}$$

and

*Present address: Department of Anatomy, FGG, Neuro-science Institute, Erasmus University Rotterdam, Postbox 1738, 3000DR Rotterdam, The Netherlands. Email address: kistler@anat.fgg.eur.nl

$$S(\boldsymbol{r},t)=\delta[V(\boldsymbol{r},t)-\vartheta]\left[\frac{\partial}{\partial t}V(\boldsymbol{r},t)\right]_+, \tag{5}$$

for all $t\in\mathbb{R}$ and $\boldsymbol{r}\in\mathbb{Z}^2$.

In order to simplify the forthcoming analysis we would like to have both V and S being defined for all points $\boldsymbol{r}\in\mathbb{R}^2$. The above equations show that there is indeed a natural extension of V and S, if we drop the restriction $\boldsymbol{r}\in\mathbb{Z}^2$ so as to obtain an *interpolated* version of both functions for $\boldsymbol{r}\in\mathbb{R}^2$.

Up to now we have not made any approximations; Eqs. (4) and (5) evaluated at $\boldsymbol{r}\in\mathbb{Z}^2$ are still exact. In order to proceed further, we introduce a continuum approximation which consists of the replacement of the discrete sum over all neurons j by an integral over space,

$$V(\boldsymbol{r},t)=\int_{\mathbb{R}^2}d^2\boldsymbol{r}'J(\|\boldsymbol{r}-\boldsymbol{r}'\|)\int_{-\infty}^{t}dt'\,\epsilon(t-t')S(\boldsymbol{r}',t') + \int_{-\infty}^{t}dt'\,\eta(t-t')S(\boldsymbol{r},t'). \tag{6}$$

This approximation is valid, if the characteristic length scale of the coupling function J is large as compared to the mesh size of the grid, i.e., if $\rho_2>\rho_1\gg 1$. Note that the present derivation of the continuum equations leads to a normalization of the δ-functions *in time*, which is different from the normalization used in [8] and [12] (see Refs. [11] and [12] for a discussion of the normalization issue).

Simulations of the underlying discrete network show that this system exhibits a large variety of dynamical patterns such as traveling wave trains, rotating spirals, and expanding target patterns [8,16,17]—a phenomenology which is very similar to that of RD systems [18]. The analysis of these patterns in the context of RD systems is often hampered by mathematical difficulties that are typical for nonlinear partial differential equations. The dynamical system defined by Eqs. (5) and (6), however, allows for a surprisingly comprehensive analytical investigation as sketched below.

We start with an analysis of a solitary traveling wave. If we substitute an ansatz for a plane wave propagating with velocity $v>0$ in positive x-direction,

$$S(x,y,t)=\delta(t-x/v), \tag{7}$$

into Eq. (6), we can calculate the corresponding membrane potentials $V(\boldsymbol{r},t)$. Equation (5) imposes a self-consistency condition on the ansatz, in the sense that the membrane potential at the position of the wave front has to be equal to the firing threshold ϑ, i.e.,

$$\vartheta=\int_{-\infty}^{\infty}dy\int_{0}^{\infty}dx\,J[\|\boldsymbol{r}\|]\epsilon(x/v), \tag{8}$$

with $\boldsymbol{r}=(x,y)$; cf. [8,9]. Note that the afterpotential η does not show up in this expression because each neuron is firing only once. Equation (8) is a relation for the propagation velocity v and the firing threshold ϑ consisting of a high- and a low-velocity branch; cf. Fig. 1.

In a similar way we can also study the properties of a periodic arrangement of traveling waves. Using the ansatz

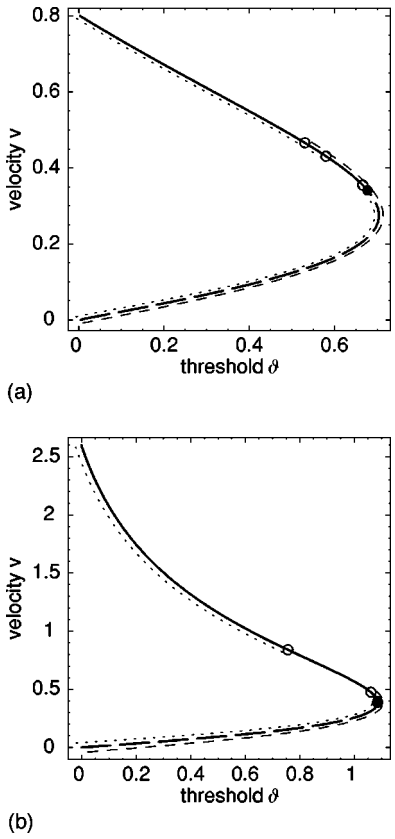

FIG. 1. Propagation velocity v of a single plane front as a function of the firing threshold ϑ (thick line). The long-dashed part of this line indicates solutions that are unstable with respect to instabilities with $\kappa_y=0$. These instabilities show up in a one-dimensional setup as well. Thin dashed or dotted lines mark the domain of instabilities that show up only in two or more dimensions, i.e., form instabilities with $\kappa_y>0$; dots correspond to perturbations with $\mathrm{Im}(c)=0$ and dashes to Hopf-instabilities with $\mathrm{Im}(c)>0$. The filled circle marks the position of the bifurcation with $\kappa_y=0$; open circles those with $\kappa_y>0$. (a) Parameters for the coupling function $\rho_1^2=15$, $\rho_2^2=100$, $a_1=1.2$, and $a_2=0.2$; cf. Eq. (3). Time constant of the postsynaptic potential $\tau=4$. (b) Similar plot as in A, but with $a_1=1.1$ and $a_2=0.1$. Note that there is a small interval between $v=0.475$ and $v=0.840$ that corresponds to fronts that are stable with respect to the perturbations considered.

$$S(x,y,t)=\sum_{n=-\infty}^{\infty}\delta[t-(x-n\lambda)/v] \tag{9}$$

and exploiting the fact that Eq. (6) is linear in the spikes, we can easily calculate the corresponding distribution of the membrane potentials. With this ansatz the neurons are firing periodically so that a contribution of the afterpotential may become important. Nevertheless, we will neglect this contribution in order to avoid a further increase in the number of free parameters. There is no harm in doing so since the afterpotential depends on the firing frequency only and the results can thus be corrected with the benefit of hindsight by rescaling the dispersion relation [8].

The self-consistency condition relates the free parameters of the ansatz, viz. wavelength λ and phase velocity v, to the firing threshold. For fixed threshold we thus obtain a dispersion relation in terms of spatial ($k=2\pi/\lambda$) and temporal frequencies ($\omega=2\pi v/\lambda$) [8],

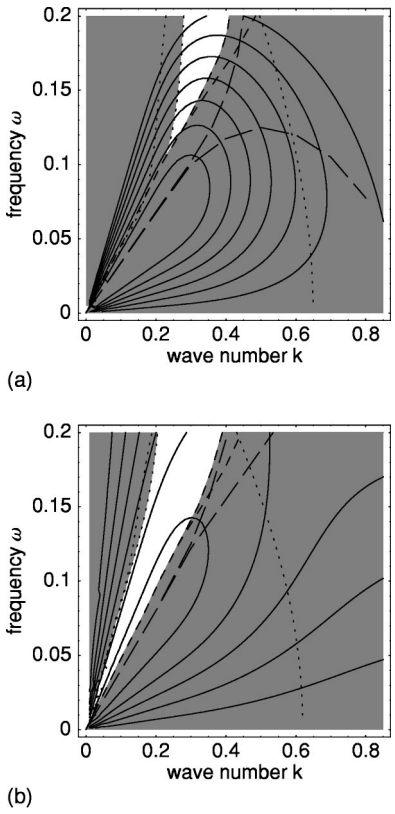

FIG. 2. (a) Dispersion relation (solid lines) of periodic wave trains for various values of the threshold parameter $\vartheta=0$ (uppermost trace), 0.1, ... , 0.6 (center). Network parameters as in Fig. 1(a). The shading indicates solutions that are unstable with respect to perturbations with $\kappa_n\in\{0,\pi\}$; cf. Eq. (13). The unshaded (white) region is bounded to the left by a form instability with $\kappa_n=0$ and $\kappa_y>0$ (dots). Its right border (dashes) is formed by a Hopf bifurcation with $\kappa_n=\pi$ and $\kappa_y>0$. The right branch of this curve corresponds to the same type of bifurcation but with $\kappa_n=0$. The remaining dotted lines to the left and to the right indicate form instabilities with $\kappa_n=\pi$. The long-dashed lines reflect bifurcations with $\kappa_y=0$, i.e., bifurcations that would show up in the corresponding one-dimensional setup. (b) Similar plot as in a but with a coupling function as in Fig. 1(b). The firing threshold varies from $\vartheta=0$ (leftmost trace) to $\vartheta=1.0$ (center) in steps of 0.2.

$$\vartheta=\sum_{n=-\infty}^{\infty}\int_{\mathbb{R}^2}d^2\boldsymbol{r}\,J(\|\boldsymbol{r}\|)\,\epsilon[(kx-2\pi n)/\omega], \tag{10}$$

with $\boldsymbol{r}=(x,y)$; cf. Fig. 2.

The stability of solutions of Eqs. (5) and (6) is investigated in terms of the neuronal firing time; cf. Ref. [11]. In the case of a solitary wave we add a small perturbation $u(x,y)$ to the firing time $T(x,y)\equiv x/v$ and substitute $S(x,y,t)=\delta[t-T(x,y)-u(x,y)]$ into Eq. (6). After linearization in $u(x,y)$ the self-consistency condition for the perturbed wave leads to a Fredholm integral equation for the perturbation,

$$0=\int_{\mathbb{R}^2}d^2\boldsymbol{r}'\,J(\|\boldsymbol{r}-\boldsymbol{r}'\|)\,\dot{\epsilon}[(x-x')/v][u(\boldsymbol{r})-u(\boldsymbol{r}')], \tag{11}$$

with $\boldsymbol{r}=(x,y)$ and $\boldsymbol{r}'=(x',y')$. The dot on the ϵ kernel denotes derivation with respect to the argument.

While performing a linear stability analysis we concentrate on a single Fourier component of the perturbation, e.g., on

$$u(x,y)=\exp(cx)\cos(\kappa_y y), \tag{12}$$

so that the integrals in Eq. (11) can be carried out. The above ansatz for the perturbation in terms of the firing time is of course not the most general one because we have restricted ourself to perturbations that travel with the same velocity as the front. Rigorous statements regarding the overall stability of the wave are therefore not possible. Nevertheless, a particular solitary wave is *unstable* if Eq. (11) can be solved by (12) with $\mathrm{Re}(c)>0$.

Figure 1 shows the propagation velocity as a function of the firing threshold together with the results of the linear stability analysis. We first looked for instabilities with $\kappa_y=0$, i.e., for instabilities that do not affect the form of the wave. This type of instability shows up in a one-dimensional setup as well. We find that the low-velocity branch is unstable because of a Hopf bifurcation close to the knee of the v-ϑ curve (long dashed line in Fig. 1). The same result was obtained by Bressloff for a one-dimensional system of integrate-and-fire neurons [11].

In a two-dimensional system we expect that instabilities play an important role that tend to bend the initially plane wave front. In fact, the present system exhibits several form instabilities ($\kappa_y>0$) that are genuine to the two-dimensional setup. The most important one destabilizes the high-velocity branch through a bifurcation slightly above the knee of the v-ϑ curve; cf. Fig. 1. Other form instabilities affect the low-velocity branch through $\mathrm{Im}(c)=0$ and Hopf bifurcations as well. Depending on the remaining free parameters that describe the shape of the coupling function the domains of the high- and the low-velocity instability may overlap so that none of the waves is stable [Fig. 1(a)]. At most, there is a narrow interval for the firing threshold that allows plane solitary waves to be stable [Fig. 1(b)].

In order to investigate the stability of the periodic wave train we consider small perturbations $u_n(\boldsymbol{r})$ added to the nth firing time $T_n(\boldsymbol{r})$ of a neuron located at position $\boldsymbol{r}$,

$$T_n(x,y)=(x-n\lambda)/v+u_n(x,y). \tag{13}$$

If we proceed as before we finally obtain a set of equations for the perturbations,

$$0=\sum_{n=-\infty}^{\infty}\int_{\mathbb{R}^2}d^2\boldsymbol{r}'\,J(\|\boldsymbol{r}-\boldsymbol{r}'\|)[u_m(\boldsymbol{r})-u_n(\boldsymbol{r}')]\times\dot{\epsilon}[(x-x'+n\lambda-m\lambda)/v], \tag{14}$$

with $m\in\mathbb{Z}$. To be specific, we consider perturbations of the form

$$u_n(x,y)=\exp[c(x-n\lambda)]\cos(\kappa_n n)\cos(\kappa_y y), \tag{15}$$

with $\kappa_n=0$ (perturbations on neighboring fronts in phase) or $\kappa_n=\pi$ (opposite phase) which results in a reduction of the system (14) to a single linearly independent equation.

Figure 2 summarizes the result of the linear stability analysis. The area below and to the right of the two long-dashed lines is found to be unstable with respect to perturbations with $\kappa_y = 0$. This would be the result of a linear stability analysis in the corresponding one-dimensional system. In two dimensions, however, the wave train is challenged by instabilities with $\kappa_y > 0$ that deviate from the planar form of the waves. These form instabilities severely restrict the domain of stable wave trains in the dispersion relation; cf. the shading in Fig. 2. Interestingly, there is a region in the dispersion relation of Fig. 2(a) that corresponds to wave trains that are stable (with respect to the considered perturbations) though all individual traveling waves are unstable; cf. Fig. 1(a). Individual waves in a wave train thus seem to stabilize each other.

In this article we have studied properties of traveling waves in a two-dimensional network that is supposed to be a simplistic model of the virtually two-dimensional architecture of the cortex. It turned out that stability properties in two dimensions are much more complex than those of the corresponding one-dimensional system. The success of the present analysis is due to the use of a pure threshold nonlinearity in Eq. (5). It has been shown previously that a certain type of nonlinear differential equation can be faithfully mapped on a response kernel formalism plus threshold-nonlinearity [15]. This formalism has been used here to describe a single neuron. Forthcoming work will show whether it is possible to use this technique in order to establish a relation between the present type of model and RD systems [18] so as to gain further insight into both.

[1] R. D. Traub, J. G. R. Jefferys, and R. Miles, J. Physiol. (London) **472**, 267 (1993).
[2] D. Golomb, Xiao-Jing Wang, and J. Rinzel, J. Neurophysiol. **75**, 750 (1996).
[3] J. Rinzel, D. Terman, X.-J. Wang, and B. Ermentrout, Science **279**, 1351 (1998).
[4] H. R. Wilson and J. D. Cowan, Kybernetik **13**, 55 (1973).
[5] S. I. Amari, Biol. Cybern. **27**, 77 (1977).
[6] G. B. Ermentrout and J. D. Cowan, Biol. Cybern. **34**, 137 (1979).
[7] M. A. P. Idiart and L. F. Abbott, Network **4**, 285 (1993).
[8] W. M. Kistler, R. Seitz, and J. L. van Hemmen, Physica D **114**, 273 (1998).
[9] B. Ermentrout, J. Comput. Neurosci. **5**, 191 (1998).
[10] D. Golomb and G. B. Ermentrout, Proc. Natl. Acad. Sci. U.S.A. **96**, 13 480 (1999).
[11] P. C. Bressloff, Phys. Rev. Lett. **82**, 2979 (1999).
[12] D. Cremers and A. V. M. Herz (unpublished).
[13] W. Gerstner and J. L. van Hemmen, Network **3**, 139 (1992).
[14] W. Gerstner, Phys. Rev. E **51**, 738 (1995).
[15] W. M. Kistler, W. Gerstner, and J. L. van Hemmen, Neural Comput. **9**, 1015 (1997).
[16] C. Fohlmeister, W. Gerstner, R. Ritz, and J. L. van Hemmen, Neural Comput. **7**, 1046 (1995).
[17] D. Horn and I. Opher, Neural Comput. **9**, 1677 (1997).
[18] J. D. Murray, *Mathematical Biology* (Springer, Berlin, 1993).